Electric-field-assisted contact mode AFM-based nanolithography with low stiffness conductive probes

Huimin Zhou[a], Yingchun Jiang[b], Christopher Dmuchowski[b,c], Changhong Ke[b,c], Jia Deng[a*]

a. Department of Systems Science and Industrial Engineering, Binghamton University, Binghamton, NY 13902 United States

b. Department of Mechanical Engineering, Binghamton University, Binghamton, NY 13902 United States

c. Materials Science and Engineering Program, Binghamton University, Binghamton, NY 13902 United States

* Corresponding Author: jiadeng@binghamton.edu

Abstract

Electric-field-assisted atomic force microscope (E-AFM) nanolithography is a novel polymer-patterning technique that has diverse applications. E-AFM uses a biased AFM tip with conductive coatings to make patterns with little probe-sample interaction, which thereby avoids the tip wear that is a major issue for contact-mode AFM-based lithography, which usually requires a high probe-sample contact force to fabricate nanopatterns; however, the relatively large tip radius and large tip-sample separation limit its capacity to fabricate high-resolution nanopatterns. In this paper, we developed a contact mode E-AFM nanolithography approach to achieve high-resolution nanolithography of poly (methyl methacrylate) (PMMA) using a conductive AFM probe with a low stiffness (~0.16 N/m). The nanolithography process generates features by biasing the AFM probe across a thin polymer film on a metal substrate. A small constant force (0.5-1 nN) applied on the AFM tip helps engage the tip-film contact, which enhances nanomachining resolution. This E-AFM nanolithography approach enables high-resolution nanopatterning with feature width down to ~16 nm, which is less than one half of the nominal tip radius of the employed conductive AFM probes.

Keywords: Atomic force microscopy, electric field, high-resolution nanopatterning, simulation, contact mode

Introduction

For decades, the scaling theory in semiconductor and integrated circuit (IC) technology development requires novel nanolithographic methods and strategies to overcome existing resolution limitations in nanodevice manufacturing [1]. Current nanolithography can be classified into masked lithography and maskless lithography. The masked lithography, such as photolithography and nanoimprint lithography [2–4], transfers patterns using lithographic masks in high throughput. The maskless lithography, which includes electron beam lithography [5], focused ion beam milling [6], direct laser writing [7], and scanning probe lithography (SPL) [8], fabricates masks for masked lithography or directly produces prototypes or products. Electron-beam lithography is developed to pattern the electron-sensitive resist layer on a substrate by emitting a beam of accelerated electrons. Similarly, focused ion beam milling uses a focused beam of ions to strike the sample and modify the surface structure. Both the electron-beam lithography and focused ion beam milling processes are capable of creating fine features,

but are costly and have low fabrication yields [9]. In contrast to these electron and ion beam-based techniques, SPL techniques, which are based mostly on atomic force microscopy (AFM) and scanning tunneling microscopy (STM) techniques, have shown great potential to fabricate high-resolution features with unprecedented technical capabilities. They have been applied to many scientific and potential industrial applications [10,11].

Compared with other nanolithography technologies mentioned above, the cost-effective AFM lithography exhibits many advantages in process simplicity and resolution [12], and can be used to make patterns on a variety of materials [13], thanks to the unique combined scanning, manipulating and imaging capabilities of ultrasharp AFM probes with a typical tip radius below 10 nm [14,15]. It can be applied to achieve nanoscale features such as nanodots [16], nanowire [17], nanofluidics [18], and 2D/3D nanopatterns [19–23] on a variety of materials, which includes polymers [24], silicon [25], metals [26], and 2D materials [27,28]. Meanwhile, the wide usage of polymers in diverse applications such as opto/microelectronics, sensors, and data storage has promoted the innovation of polymer nanolithography [16]. Nanopatterns fabricated on the polymer film can be transferred to different substrate materials through reactive ion etching (RIE) while using the patterned polymer film as a mask [29].

AFM-based nanolithography processes rely on the interaction of AFM tips with sample substrates [30]. AFM tip-sample interactions in nanopatterning processes include mechanical-, thermal-, chemical-, and electric-induced interactions [13]. The mechanical interactions are utilized in dynamic plowing [31], direct machining [32], and vibration-assisted lithography [33,34]. Thermal-assisted AFM lithography includes thermal writing that uses a heated AFM probe [35], and a sample heating method by using a softened sample under elevated temperatures [34]. Electric-field-assisted AFM lithography, or the so-called bias-assisted AFM lithography process, involves highly confined joule heating, local oxidation, field emission, and electrostatic interactions [14,36–40].

Two typical electric-field-assisted AFM nanolithography techniques for patterning polymers are AFM-assisted electrostatic lithography (AFMEN) and field-emission scanning probe lithography (FE-SPL) [36,41,42]. AFMEN generates features through biasing a conductive AFM probe above a thin polymer film that rests on a grounded conductive film on silicon substrate. Features are formed by joule heating from the current flow between AFM tip and conductive substrate. Depending on the applied voltage, either raised features (by the effect of non-uniform electric field gradient on polarizable softened polymer) or depressed features (by polymer ablation) can be generated by AFMEN, which has an initial gap distance between an AFM tip and a sample [41]. Studies show that feature size of SPL-based electrostatic lithography is influenced by a number of factors, such as tip radius, current magnitude, and material characteristics of polymers [43]. In addition, AFM tip-polymer film separation is one of the critical factors that leads to the control of polymer dielectric breakdown [16]. As the distance between tip–polymer surface increases, larger-size pattern features are fabricated [44]. Similarly, the amplitude-modulated AFMEN (AM-AFMEN) process includes an oscillating conductive AFM tip. This process can be applied to make nanodots with smaller dimensions due to variant tip-sample interaction distance and better control of the heat generation. FE-SPL process also applies bias between a sharp AFM tip (with 7-15 nm tip radius) and the sample, which generates a Fowler–Nordheim (FN) field emission of low energy electrons and leads to the cross-linking or scission of the polymer resist sample [36]. A feedback control can be incorporated in this technique to maintain both a constant emission current through controlling tip-sample distance in the lithography process and a constant tip oscillation amplitude in regular scanning [45].

A larger distance between tip–polymer surface leads to the formation of wider nanostructures because tip-film separation acts as one of the governing factors that affect the polymer dielectric breakdown and fabricated feature size [16,44] (see Supplementary information for further details). Much of the existing literature reported electric-field-assisted AFM lithography experiments under tapping mode (or amplitude-modulated mode), in which tip-sample distance is within a large range due to the tip oscillation. Among studies that use similar nanolithography techniques, AFMEN was conducted with no tip-film contact and a tip-sample separation possibly due to condensed water meniscus between the AFM tip and the polymer film. The fabricated nanopits and nanogrooves typically have large feature width of around 500 nm [41]. AM-AFMEN fabricates nanopatterns with finer resolution; however, this process requires a more complex and precise control of cantilever oscillation amplitude, applied AFM tip bias, and tip-sample interactions. Except for the tip-sample distance, the patterning speed is another important indicator when evaluating the lithography techniques [46,47]. One of the existing SPM technologies has reached a very high patterning speed at meters per second [48].

In this study, we developed a contact mode electric-field-assisted AFM lithography process that generates high-resolution nanofeatures on polymer substrates using a soft probe. Constant force of 0.5-1 nN was applied to the AFM tip to secure the tip-film contact, in which localized electric breakdown took place inside the polymer film produced nanoholes and nanopatterns with adjustable feature dimensions. Nanostructures with feature widths down to ~16 nm were fabricated on a 15 nm-thick PMMA film, which was coated on a gold layer. Moreover, we studied the effects of applied bias voltage, contact force, and bias duration time on the lithographic feature dimensions. We also simulated the tip-induced electric field strength distributions in the polymer layer using finite element analysis. This study demonstrates a new method of fabricating high-resolution nanopatterns using contact mode electric-field-assisted AFM with a small contact force.

Methods

The contact mode electric-field-assisted AFM lithography experiments were performed inside a commercial AFM (XE7, Park Systems Corporation) with a high voltage toolkit. A schematic of the electric-field-assisted AFM lithography setup is shown in Fig. 1 (see Supplementary information for the actual experimental setup). The entire setup was placed inside an acoustic enclosure, which had a humidity of ~15%. The sample is prepared by first e-beam evaporation of an Au layer (100 nm thickness) on a silicon substrate. Subsequently, a 15 nm polymethyl methacrylate (PMMA) layer was spin-coated on the Au layer, followed by a post baking at 180 °C for 90 seconds. A conductive AFM probe (CSG10/Au) with conductive Au coatings on both the tip side and the back side was used in contact mode lithography, which applied small constant contact forces (1 nN) between the AFM tip and sample. A sharp AFM probe (MCNT-500 12 deg) was used in noncontact (tapping) mode to image the lithography results (see Supplementary information for specifications of the AFM probes).

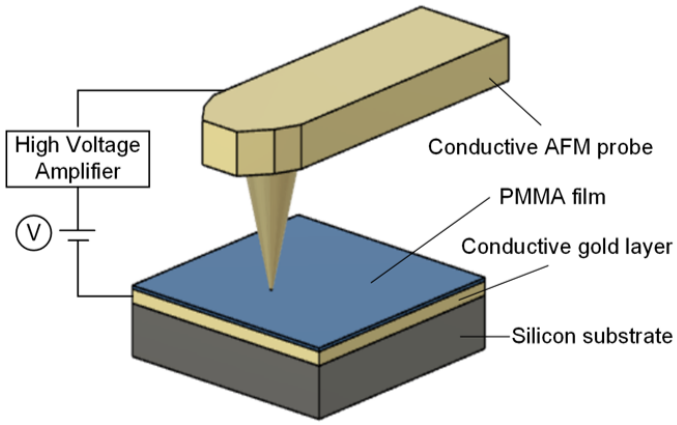

Figure 1. Schematic illustration of electric-field-assisted contact mode AFM-based nanolithography experimental setup.

Numerical simulations were conducted using ANSYS Maxwell 3D to simulate the electric-field-assisted AFM lithography process and to generate the distributions of electric field strength in the polymer film.

Experimental and simulation results

With the electric-field-assisted AFM lithography setup mentioned in the previous chapter, multiple nanopatterns with different feature dimensions were fabricated on the 15 nm-thick PMMA film. The lithography speed was set at 0.5 μm/s.

One of the most important factors in the electric-field-assisted lithography process is tip bias. Fig. 2 shows results of several experiments that were conducted to analyze the voltage effect on lithography feature dimensions. Fig. 2(a) shows three trenches fabricated with bias voltage of 32.4V, 33.3V, 34.1V, which correspond to input voltages of 1.85V, 1.90V, 1.95V before amplification, respectively. As shown in the z profile of the topography image in Fig. 2(b), the depth of the three lines is around 3.0, 4.0, and 5.0 nm, respectively. Nanopatterns in Fig. 2(d) also exhibit similar results in which the trench depth increases as the voltage increases. The voltage applied from left to right trenches are 22.93V, 21.18V, 23.10V, 21.35V, 23.28V, 21.53V, 23.45V, 21.7V, 23.63V, 21.88V, 23.8V, 22.05V, 23.98V, 22.23V, respectively. Note that the force applied on the AFM tip during lithography was set as 1nN for all the tests. Measurement results of topography images in Fig. 2(a) and 2(d) are shown in Fig. 2(b) and 2(e), respectively. Figs. 2(c) and 2(f) show a summary of the fabricated trench width and depth versus applied voltage for the nanotrenches shown in in Figs. 2(a) and 2(d). Based on the height profiles, we measured trench depths and widths in five random spots along each trench and took the average value. In Fig. 2(c), for voltage applied between 32.4 and 34.1V, trench depth ranged between 3.3 and 4.7 nm, and trench width ranged between 26 and 33 nm. In Fig. 2(f), for voltage applied between 21.18 and 23.98V, trench depth ranged between 1.1 and 3.0 nm, and trench widths ranged between 25 and 36 nm.

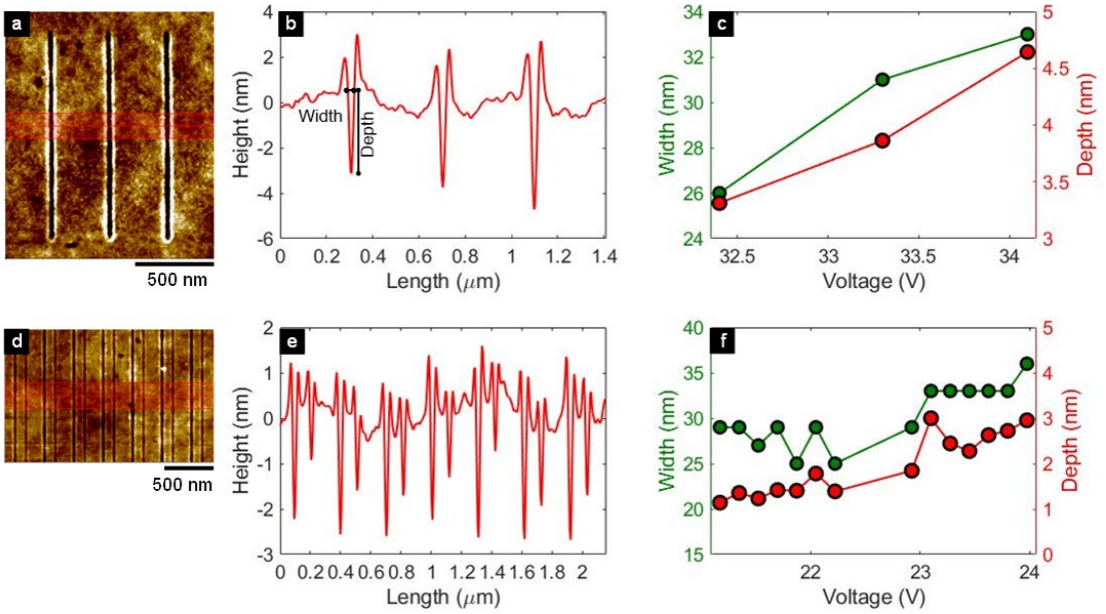

Figure 2. Voltage effect on lithography feature size. (a) Topography of lines fabricated with 32.4V, 33.3V, 34.1V, from left to right. (d) Topography of lines fabricated with voltage ranging from 22.93V, 21.18V, 23.1V, 21.35V, 23.28V, 21.53V, 23.45V, 21.7V, 23.63V, 21.88V, 23.8V, 22.05V, 23.98V, 22.23V from left to right. (b)&(e) Average height profiles of the patterns in Fig. 2(a)&(d). (c)&(f) Voltage versus feature dimensions.

In addition, we investigated the effect of tip bias hold time on the lithography dimensions. Fig. 3(a) shows the 2D image of holes fabricated in electric-field-assisted contact mode AFM-based nanolithography, in which the tip bias hold time was set as 100 ms, 160 ms, 220 ms, respectively, with 1nN contact force and 24 V tip bias applied for all three holes. Fig. 3(b) is a depth-profile view of the fabricated holes, which shows the depth differences of the three holes. Depths of holes increase from 5.3 nm to 11.0 nm, and widths increase from ~27 nm to ~33 nm, as the tip bias duration increases from 100 ms to 220 ms, as shown in Fig. 3(c). The results demonstrate the effect of bias hold time on the dimensions of holes.

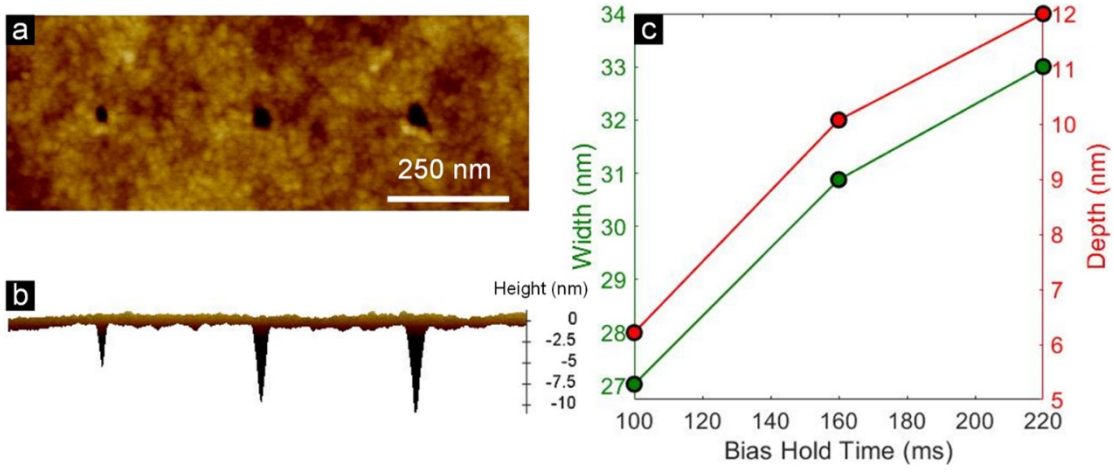

Figure 3. Tip bias hold time effect on feature sizes. (a) 2D image of holes fabricated using electric-field-assisted contact mode AFM-based nanolithography. Tip bias applied was 24 V and bias hold time was 100 ms, 160 ms, 220 ms, respectively. (b) Front view of the 3D image of the holes, depths of the three holes are 5.3 nm, 8.9 nm, 11.0 nm, and widths are ~27 nm, ~31 nm, and ~33 nm, respectively. (c) Bias hold time versus dimensions of holes.

We conducted another experiment to investigate the effect of normal force applied by the AFM tip on the dimensions of features in the lithography process. As shown below in Fig. 4(a), the designed pattern includes two NSF logos, in which the characters of NSF are inside an ellipse. We set the contact force of the NSF characters in the left circle to be 1 nN, which is a very small load force simply to ensure the contact between AFM tip and sample. To make a better comparison of different forces, we applied 8 nN to NSF characters in the right circle. The tip was applied with an 8 nN contact force in drawing the two circles.

As shown in Fig. 4(b), height profiles of the left and right NSF logos show similar patterns but with different feature depths. The maximum depth of the left NSF characters fabricated with 1 nN force was about 2.5 nm, while it was about 8.0 nm for the right NSF characters fabricated with 8 nN force. Therefore, the contact force has a substantial influence on the size of the feature patterned by using electric-field-assisted contact mode AFM-based nanolithography. An increase in the contact force results in an increase in feature width. However, as the contact force between the tip and sample becomes larger, it leads to larger tip wear. The resulting tip apex dimension change and reduction of the conductive coating on the AFM tip might negatively affect the lithographic performance.

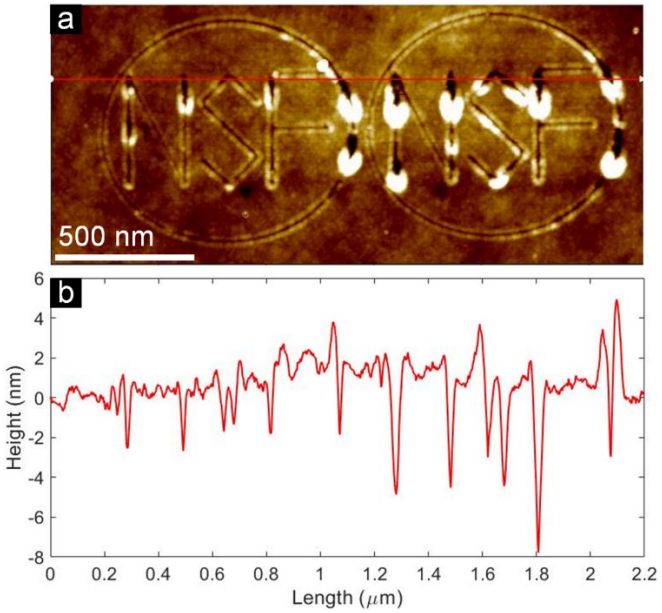

Figure 4. Force effect on lithography feature sizes. (a) Topography of NSF logos fabricated with 1 nN and 8 nN setpoint force with the same applied bias (20V). (b) Height profile of patterns in Fig. 4(a).

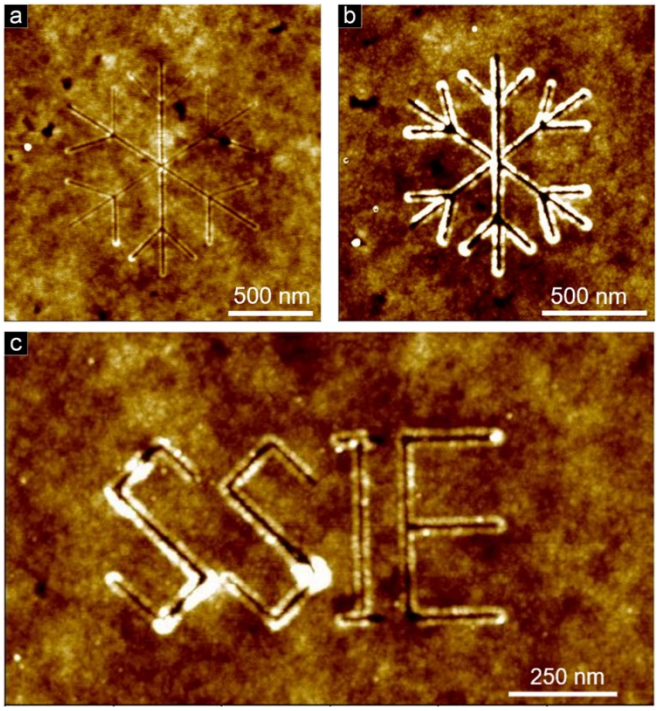

Figure 5. Nanopatterns fabricated with electric-field-assisted AFM lithography. Applied force is 1 nN for all the patterns.

Fig. 5 shows several nanopatterns that include snowflake shapes and SSIE characters. The two snowflake patterns are fabricated with 1 nN setpoint force and a tip bias of 17.50 and 26.25 V, respectively, which correspond to input voltages of 1.0 and 1.5 V, respectively. Patterns in Fig. 5(a) have a feature depth around 0.5-1 nm and a trench width around 16-30 nm. Feature depths for the nanopatterns in (b) and (c) are around 1-2 nm.

Because the applied mechanical force in our E-AFM lithography is small, the observed debris along the side of fabricated features is assumed to be produced mainly by the effect of electrostatic force from a non-uniform electric field gradient on softened or melted polymer, which is on the outside of the sublimated polymer. The direction of the electrostatic force on the polarized softened or melted polymer is towards the tip end; therefore, raised debris on the trench side appears. Even so, the debris alongside the fabricated patterns is much less than that produced by other mechanical force-based AFM lithography techniques.

As it is an important parameter to evaluate the lithography performance, we also studied the effect of lithography speed on the patterning results. We designed four lines with 400 nm interval between each other. The patterns were fabricated with different lithography speeds (50, 10, 5, 0.5 μm/s from left to right, respectively). Measurement shows the trench width of the four lines from left to right are 0, ~25, ~28, ~32 nm, and the trench depths are 0, 1.35, 1.79, 2.95 nm, respectively. The results show that feature depth gradually increases as patterning speed decreases. As the results in Figure 2 indicate that deeper trenches can be fabricated through the increase of tip bias voltage, we could potentially achieve higher nanopatterning speed by applying higher voltages to compensate the reduced feature depths of higher machining speed.

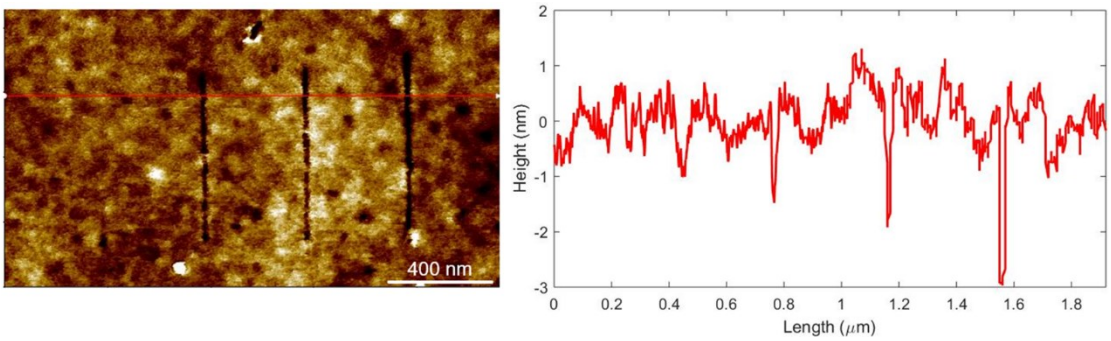

Figure 6. Nanopatterns fabricated with electric-field-assisted AFM lithography in different speeds (50, 10, 5, 0.5 μm/s from left to right, respectively). Applied force is 1 nN for all the patterns.

To understand the effect of the electric field strength on the nanolithography results, we developed a simulation model in ANSYS Electronics and performed some quantitative analysis on the electric-field-assisted contact mode AFM-based nanolithography, as shown in Fig. 7(a). The model is composed of a gold sphere with 35 nm radius, which is the size of the AFM tip end. The gold sphere is in contact with a 15-nm thick PMMA film, which is on the top of a 100 nm thick gold layer. To better study the distribution of electric field strength in the polymer layer, we inserted six lines (Line 0, 1, 2, 3, 5, and 6) on the Y-Z plane inside the PMMA film, which has z values equal to 0, -3, -6, -9, and -12 nm, respectively. These lines evenly divided the polymer film into five 3 nm regions on the Y-Z plane. Line 6 was designed as a line on Z-axis in the PMMA film to show the electric-field changes in the z-direction. We set the simulation temperature as 22 degrees Celsius, which is close to the actual temperature. Tip bias was defined by assigning a voltage excitation on the sphere, while the voltage applied to the gold layer was 0 V.

Fig. 7(b) shows the electric field distribution on the Y-Z plane in the PMMA film with an applied 20 V tip bias, where the maximum electric field strength is around 2×10^9 V/m, which is located at the tip-film interface right under the AFM tip. With the same applied tip bias, Fig. 7(c) shows the electric field strength distribution on Line 1-5 designed in Fig. 7(a). Each of them has a bell-shaped curve, the maximum electric field strength increases from 1×10^9 V/m to 2.5×10^9 V/m as the line gets closer to the X-Y plane. Based on the simulation results, for the experiments that generate features with 16 nm width, the relative electric field strength is around 1.63×10^9 V/m (plotted Fig. 7(c) in dash lines). Fig. 7(d) shows the electric field strength distribution on Line 6 (along the Z-axis). As the distance from the tip-film interface increases, the electric field strength gradually decreases.

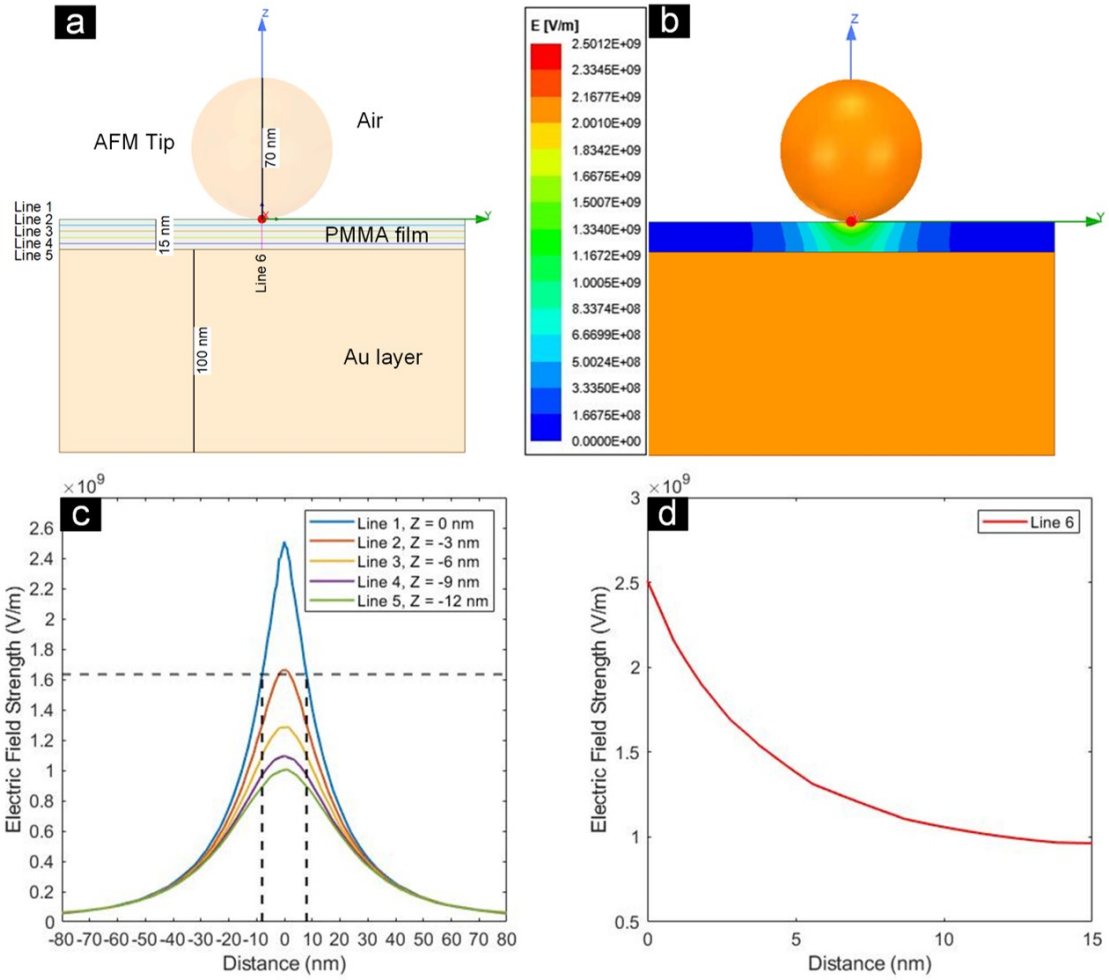

Figure 7. Electric field strength distribution in the polymer film during lithography (applied tip bias = 20V). (a) Front view of the simulation model, including the location of Line 1-6. (b) Electric field distribution in the PMMA film. (c) Electric field distribution on Line 1-5. Based on the experimental results, which have feature width of around 16 nm, the relative electric field strength on the tip-sample interface (Line 1) should reach or exceed $1.63 \times 10^9\ V/m$. (d) Electric field distribution along Line 6.

To explore the potential of fabricating sub-10 nm feature sizes, we changed two major factors in the simulation model that may affect the nanolithography resolution: tip radius and PMMA film thickness. Fig. 8 shows the simulation results with the same tip bias of 20 V while changing the tip radius and PMMA film thickness. In Fig. 8(a), we show the electric field strength distributions on the tip-sample interface along the Y-axis for the cases of four different tip radii (20, 10, 5, and 3 nm), while the PMMA film thickness was 15 nm. According to our previous experimental and simulation results in Fig. 7(c), features with 16 nm width corresponds to the electric field strength of $1.63 \times 10^9\ \mathrm{V/m}$. Using this value as the threshold to fabricate nanopatterns, the simulation results in Fig. 8(a) indicate that the feature width can be reduced to sub-10 nm (9.2 nm) if we use an AFM tip with 3 nm radius. A tip with 20 nm radius results in a feature width of 14.8 nm. Results show that feature width decreases along with the decrease of tip radius, which indicates a great potential to fabricate nanopatterns with sub-10 nm resolution if a sharp tip in the electric-field-assisted contact mode AFM-based nanolithography is used.

Fig. 8(b) shows electric field strength distributions along the Y-axis for the cases of different film thickness, which are 10, 15, 20, and 30 nm, while the tip radius is 35 nm and tip bias is 20 V. Results show the minimum feature width is 6 nm when the thick PMMA film thickness is 30 nm, and the feature width is 20.6 nm when the thin PMMA film thickness is 10 nm. Results

indicate that finer features could be fabricated on thicker PMMA film if other factors remain the same. The reason is that the critical electric field strength crosses a short distance on the thicker film compared to that on the thinner film. However, the electric field strength shows a greater slop on the thin film, which could be beneficial to the edge sharpness of fabricated nanopatterns. The tip bias can be set at a lower level in experiments to reach the critical electric field strength if on thinner films. Therefore, thinner film thickness is preferred in nanolithography processes that aim to fabricate nanopatterns with sharper edges.

Comparing the effects of two factors, tip radius and film thickness, on the nanolithography resolution, reducing tip radius has greater potential to improve the nanolithography resolution and quality. A sharp increase in the electric field strength distribution using a tip with a small radius could greatly lower the needed tip bias and could potentially sharpen the edges of nanopatterns, which leads to high-resolution and high-quality nanopatterns.

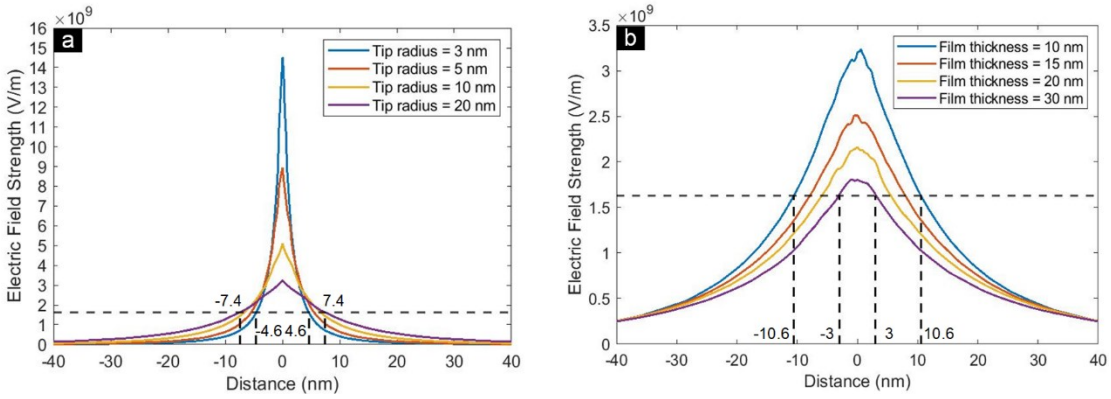

Figure 8. Electric field strength distributions on the tip-sample interface (along the Y-axis) using 20 V tip bias with (a) different tip radii of 3, 5, 10, and 20 nm when PMMA film thickness is 15 nm, and (b) different PMMA film thicknesses of 10, 15, 20, and 30 nm using a tip with 35 nm radius.

Conclusions

In summary, we demonstrated a novel method of fabricating high-resolution nanopatterns using contact mode electric-field-assisted AFM lithography, which fabricates fine features with little debris on a thin polymer film using very small contact force. The experiments were conducted with direct gentle tip-sample contact. Through the application of a different tip bias, contact force applied on the tip, and tip bias hold time, we fabricated high-resolution nanofeatures that included holes, trenches, and other nanopatterns with feature widths down to ~16 nm. We studied the effects of several process parameters, which included tip bias, contact force, and bias hold time on the dimensions of nanopatterns to better control the lithography performance in the actual experiments. Moreover, we developed a numerical simulation model to analyze the tip bias-induced electric field strength distribution in the polymer film. The simulation results provided more quantitative insights into the process mechanism and the future research directions to enhance the resolution and quality of nanopatterns. The contact mode electric-field-assisted AFM-based nanopatterning process developed in this paper shows great potential in fabricating nanopatterns with sub-10 nm resolution, which can advance nanomanufacturing fields and nano-enabled scientific and industrial applications.

Acknowledgments

This work was supported in part by the National Science Foundation under grant no. CMMI-2006127, and by the Small Scale Systems Integration and Packaging (S3IP) Center of Excellence, funded by the New York Empire State Development's Division of Science, Technology, and Innovation.

References

[1] M. Kaestner, I.W. Rangelow, Scanning probe nanolithography on calixarene, Microelectron. Eng. 97 (2012) 96–99. https://doi.org/10.1016/j.mee.2012.05.042.

[2] Z. Sekkat, S. Kawata, Laser nanofabrication in photoresists and azopolymers, Laser Photonics Rev. 8 (2014) 1–26. https://doi.org/10.1002/lpor.201200081.

[3] C.A. Mack, Reducing roughness in extreme ultraviolet lithography, in: Int. Conf. Extreme Ultrav. Lithogr. Monterey, California, United States. 11-14 September 2017, International Society for Optics and Photonics, 2017: p. 104500P. https://doi.org/10.1117/12.2281605.

[4] A. Pimpin, W. Srituravanich, Review on Micro- and Nanolithography Techniques and Their Applications, Eng. J. 16 (2012) 37–56. https://doi.org/10.4186/ej.2012.16.1.37.

[5] J.A. Lee, K.-C. Lee, S.I. Park, S.S. Lee, The fabrication of carbon nanostructures using electron beam resist pyrolysis and nanomachining processes for biosensing applications, Nanotechnology. 19 (2008) 215302. https://doi.org/10.1088/0957-4484/19/21/215302.

[6] F. Watt, A.A. Bettiol, J.A. Van Kan, E.J. Teo, M.B.H. Breese, Ion beam lithography and nanofabrication: a review, Int. J. Nanosci. 04 (2005) 269–286. https://doi.org/10.1142/S0219581X05003139.

[7] L. Li, M. Hong, M. Schmidt, M. Zhong, A. Malshe, B. Huis in'tVeld, V. Kovalenko, Laser nano-manufacturing – State of the art and challenges, CIRP Ann. 60 (2011) 735–755. https://doi.org/10.1016/j.cirp.2011.05.005.

[8] A.A. Tseng, A. Notargiacomo, T.P. Chen, Nanofabrication by scanning probe microscope lithography: A review, J. Vac. Sci. Technol. B Microelectron. Nanometer Struct. Process. Meas. Phenom. 23 (2005) 877–894. https://doi.org/10.1116/1.1926293.

[9] C. Duan, W. Wang, Q. Xie, Review article: Fabrication of nanofluidic devices, Biomicrofluidics. 7 (2013) 026501. https://doi.org/10.1063/1.4794973.

[10] M. Kaestner, T. Ivanov, A. Schuh, A. Ahmad, T. Angelov, Y. Krivoshapkina, M. Budden, M. Hofer, S. Lenk, J.-P. Zoellner, I.W. Rangelow, A. Reum, E. Guliyev, M. Holz, N. Nikolov, Scanning probes in nanostructure fabrication, J. Vac. Sci. Technol. B. 32 (2014) 06F101. https://doi.org/10.1116/1.4897500.

[11] Y.K. Ryu Cho, C.D. Rawlings, H. Wolf, M. Spieser, S. Bisig, S. Reidt, M. Sousa, S.R. Khanal, T.D.B. Jacobs, A.W. Knoll, Sub-10 Nanometer Feature Size in Silicon Using Thermal Scanning Probe Lithography, ACS Nano. 11 (2017) 11890–11897. https://doi.org/10.1021/acsnano.7b06307.

[12] M. Behzadirad, A.K. Rishinaramangalam, D. Feezell, T. Busani, C. Reuter, A. Reum, M. Holz, T. Gotszalk, S. Mechold, M. Hofmann, A. Ahmad, T. Ivanov, I.W. Rangelow, Field emission scanning probe lithography with GaN nanowires on active cantilevers, J. Vac. Sci. Technol. B. 38 (2020) 032806. https://doi.org/10.1116/1.5137901.

[13] R. Garcia, A.W. Knoll, E. Riedo, Advanced scanning probe lithography, Nat. Nanotechnol. 9 (2014) 577–587. https://doi.org/10.1038/nnano.2014.157.

[14] R. Garcia, R.V. Martinez, J. Martinez, Nano-chemistry and scanning probe nanolithographies, Chem. Soc. Rev. 35 (2006) 29–38. https://doi.org/10.1039/b501599p.

[15] A. Michalek, T. Jwad, P. Penchev, T.L. See, S. Dimov, Inline LIPSS Monitoring Method Employing Light Diffraction, J. Micro Nano-Manuf. 8(1) (2020) 011002. https://doi.org/10.1115/1.4045681.

[16] S.F. Lyuksyutov, P.B. Paramonov, S. Juhl, R.A. Vaia, Amplitude-modulated electrostatic nanolithography in polymers based on atomic force microscopy, Appl. Phys. Lett. 83 (2003) 4405–4407. https://doi.org/10.1063/1.1629787.

[17] S.D. Hutagalung, K. Lew, T. Darsono, Nanoscale Patterning by AFM Lithography and its Application on the Fabrication of Silicon Nanowire Devices, Sains Malays. 43 (2014) 267–272. http://www.ukm.my/jsm/pdf_files/SM-PDF-43-2-2014/15%20Sabar%20D.%20Hutagalung.pdf

[18] R. Promyoo, H. El-Mounayri, M. Agarwal, V.K. Karingula, K. Varahramyan, Tip-Based Nanomanufacturing of Nanofluidics Using Atomic Force Microscopy, J. Micro Nano-Manuf. 4(4) (2016) 041003. https://doi.org/10.1115/1.4034608.
[19] H. Zhou, J. Deng, Vibration Assisted AFM-Based Nanomachining under Elevated Temperatures using Soft and Stiff Probes, Procedia Manuf. 48 (2020) 508–513. https://doi.org/10.1016/j.promfg.2020.05.075.
[20] J. Deng, L. Zhang, J. Dong, P.H. Cohen, AFM-based 3D nanofabrication using ultrasonic vibration assisted nanomachining, J. Manuf. Process. 24 (2016) 195–202. https://doi.org/10.1016/j.jmapro.2016.09.003.
[21] Y. Geng, Y. Yan, E. Brousseau, Y. Sun, AFM tip-based mechanical nanomachining of 3D micro and nano-structures via the control of the scratching trajectory, J. Mater. Process. Technol. 248 (2017) 236–248. https://doi.org/10.1016/j.jmatprotec.2017.05.028.
[22] Y. Geng, Y. Yan, J. Wang, E. Brousseau, Y. Sun, Y. Sun, Fabrication of Periodic Nanostructures Using AFM Tip-Based Nanomachining: Combining Groove and Material Pile-Up Topographies, Engineering. 4 (2018) 787–795. https://doi.org/10.1016/j.eng.2018.09.010.
[23] E.B. Brousseau, S. Thiery, B. Arnal, E. Nyiri, O. Gibaru, J.R. Mayor, A Computer-Aided Design and Manufacturing Implementation of the Atomic Force Microscope Tip-Based Nanomachining Process for Two-Dimensional Patterning, J. Micro Nano-Manuf. 5(4) (2017) 041003. https://doi.org/10.1115/1.4037694.
[24] H. Liu, S. Hoeppener, U.S. Schubert, Reversible Nanopatterning on Polypyrrole Films by Atomic Force Microscope Electrochemical Lithography, Adv. Funct. Mater. 26 (2016) 614–619. https://doi.org/10.1002/adfm.201503834.
[25] S.F. Lyuksyutov, P.B. Paramonov, I. Dolog, R.M. Ralich, Peculiarities of an anomalous electronic current during atomic force microscopy assisted nanolithography on n-type silicon, Nanotechnology. 14 (2003) 716–721. https://doi.org/10.1088/0957-4484/14/7/305.
[26] L. Zhang, J. Dong, P.H. Cohen, Material-Insensitive Feature Depth Control and Machining Force Reduction by Ultrasonic Vibration in AFM-Based Nanomachining, IEEE Trans. Nanotechnol. 12 (2013) 743–750. https://doi.org/10.1109/TNANO.2013.2273272.
[27] X. Liu, S.T. Howell, A. Conde-Rubio, G. Boero, J. Brugger, Thermomechanical Nanocutting of 2D Materials, Adv. Mater. 32 (2020) 2001232. https://doi.org/10.1002/adma.202001232.
[28] H. Bark, S. Kwon, C. Lee, Bias-assisted atomic force microscope nanolithography on NbS2thin films grown by chemical vapor deposition, J. Phys. Appl. Phys. 49 (2016) 484001. https://doi.org/10.1088/0022-3727/49/48/484001.
[29] J. Deng, J. Dong, P. Cohen, Rapid Fabrication and Characterization of SERS Substrates, Procedia Manuf. 26 (2018) 580–586. https://doi.org/10.1016/j.promfg.2018.07.068.
[30] H. Hu, H.J. Kim, S. Somnath, Tip-Based Nanofabrication for Scalable Manufacturing, Micromachines. 8 (2017). https://doi.org/10.3390/mi8030090.
[31] B. Klehn, U. Kunze, Nanolithography with an atomic force microscope by means of vector-scan controlled dynamic plowing, J. Appl. Phys. 85 (1999) 3897–3903. https://doi.org/10.1063/1.369761.
[32] T.-H. Fang, W.-J. Chang, Effects of AFM-based nanomachining process on aluminum surface, J. Phys. Chem. Solids. 64 (2003) 913–918. https://doi.org/10.1016/S0022-3697(02)00436-5.
[33] J. Deng, J. Dong, P.H. Cohen, Development and Characterization of Ultrasonic Vibration Assisted Nanomachining Process for Three-Dimensional Nanofabrication, IEEE Trans. Nanotechnol. 17 (2018) 559–566. https://doi.org/10.1109/TNANO.2018.2826841.
[34] H. Zhou, C. Dmuchowski, C. Ke, J. Deng, External-energy-assisted nanomachining with low-stiffness atomic force microscopy probes, Manuf. Lett. 23 (2020) 1–4. https://doi.org/10.1016/j.mfglet.2019.11.001.

[35] F. Holzner, P. Paul, M. Despont, L.L. Cheong, J. Hedrick, U. Dürig, A. Knoll, Thermal probe nanolithography: in-situ inspection, high-speed, high-resolution, 3D, in: 29th Eur. Mask Lithogr. Conf., International Society for Optics and Photonics. Dresden, Germany. 25 June 2013: p. 888605. https://doi.org/10.1117/12.2032318.
[36] M. Kaestner, I.W. Rangelow, Scanning probe lithography on calixarene towards single-digit nanometer fabrication, Int. J. Extreme Manuf. 2 (2020) 032005. https://doi.org/10.1088/2631-7990/aba2d8.
[37] L. Ding, Y. Li, H. Chu, C. Li, Z. Yang, W. Zhou, Z.K. Tang, High speed atomic force microscope lithography driven by electrostatic interaction, Appl. Phys. Lett. 91 (2007) 023121. https://doi.org/10.1063/1.2756138.
[38] Y.K. Ryu, R. Garcia, Advanced oxidation scanning probe lithography, Nanotechnology. 28 (2017) 142003. https://doi.org/10.1088/1361-6528/aa5651.
[39] C. Ovenden, I. Farrer, M.S. Skolnick, J. Heffernan, Nanoscale wafer patterning using SPM induced local anodic oxidation in InP substrates, Semicond. Sci. Technol. 37 (2021) 025001. https://doi.org/10.1088/1361-6641/ac3f20.
[40] A. Kayal, H. G, K. Bandopadhyay, A. Kumar, S.R.P. Silva, J. Mitra, Controlling the macroscopic electrical properties of reduced graphene oxide by nanoscale writing of electronic channels, Nanotechnology. 32 (2021) 175202. https://doi.org/10.1088/1361-6528/abda72.
[41] S.F. Lyuksyutov, R.A. Vaia, P.B. Paramonov, S. Juhl, L. Waterhouse, R.M. Ralich, G. Sigalov, E. Sancaktar, Electrostatic nanolithography in polymers using atomic force microscopy, Nat. Mater. 2 (2003) 468–472. https://doi.org/10.1038/nmat926.
[42] Y. Krivoshapkina, M. Kaestner, C. Lenk, S. Lenk, I.W. Rangelow, Low-energy electron exposure of ultrathin polymer films with scanning probe lithography, Microelectron. Eng. 177 (2017) 78–86. https://doi.org/10.1016/j.mee.2017.02.021.
[43] I.W. Rangelow, T. Ivanov, Y. Sarov, A. Schuh, A. Frank, H. Hartmann, J.-P. Zöllner, D.L. Olynick, V. Kalchenko, Nanoprobe maskless lithography, in: Altern. Lithogr. Technol. II, International Society for Optics and Photonics. San Jose, California, USA. 23-25 February 2010: p. 76370V. https://doi.org/10.1117/12.852265.
[44] S.F. Lyuksyutov, P.B. Paramonov, R.A. Sharipov, G. Sigalov, Induced nanoscale deformations in polymers using atomic force microscopy. American Physical Society (United States). Phys. Rev. B 70, 174110 (2004). https://doi.org/10.1103/PhysRevB.70.174110.
[45] C. Lenk, M. Hofmann, S. Lenk, M. Kaestner, T. Ivanov, Y. Krivoshapkina, D. Nechepurenko, B. Volland, M. Holz, A. Ahmad, A. Reum, C. Wang, M. Jones, Z. Durrani, I.W. Rangelow, Nanofabrication by field-emission scanning probe lithography and cryogenic plasma etching, Microelectron. Eng. 192 (2018) 77–82. https://doi.org/10.1016/j.mee.2018.01.022.
[46] W. Shim, A.B. Braunschweig, X. Liao, J. Chai, J.K. Lim, G. Zheng, C.A. Mirkin, Hard-tip, soft-spring lithography, Nature. 469 (2011) 516–520. https://doi.org/10.1038/nature09697.
[47] P.C. Paul, A.W. Knoll, F. Holzner, M. Despont, U. Duerig, Rapid turnaround scanning probe nanolithography, Nanotechnology. 22 (2011) 275306. https://doi.org/10.1088/0957-4484/22/27/275306.
[48] B. Yao, C. Chen, Z. Du, Q. Qian, L. Pan, Surfing Scanning Probe Nanolithography at Meters Per Second, Nano Lett. 22 (2022) 2187–2193. https://doi.org/10.1021/acs.nanolett.1c03705.

Supplementary information

The actual setup of the electric-field-assisted AFM lithography setup is shown in Fig. S1. And the specifications of the AFM probes for nanopatterning and imaging is listed in Table S1.

Figure S1. Actual experimental setup

Table S1. Specifications of the AFM probes for nanopatterning and imaging.

AFM probe name	Tip radius (nm)	Tip material	Force Constant (N/m)	Function
CSG10/Au	35	Si + Au coating	0.11	Lithography
MCNT-500 12 deg	5	HDC/DLC	40	Imaging

A comparison of experiments with different tip-film separation distances is shown in Fig. S2. A bias voltage is applied between the inverted-pyramid-shaped AFM tip and the substrate. The electric field strength in the AFM tip-sample gap region gradually decreases as an increase of the gap distance. Meanwhile, the initial electric field strength at the AFM tip end is also controlled by the applied AFM tip bias. For example, the electric field strength at the left AFM tip end (represented by light red color) is smaller than that at the right AFM tip end (represented by dark red color), which indicates a smaller tip bias applied on the left AFM tip. Assuming the joule heating induced by electrons emitting from the AFM tip end is large enough to initiate localized sublimating of the polymer film (covered by the lightest pink electric field strength contour), the width of the features created by the same AFM tip increases with a larger tip-sample distance.

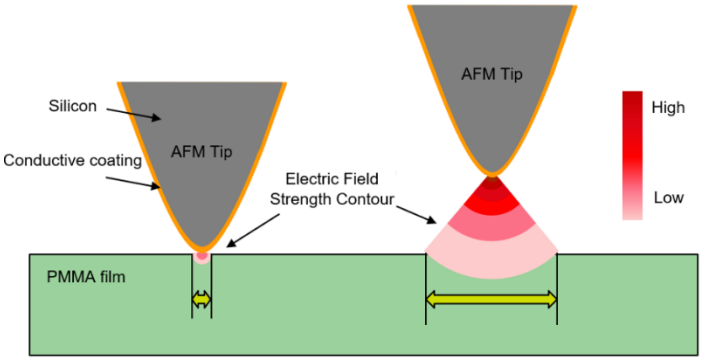

Figure S2. Illustration of the tip-sample distance effect on the minimum feature size in E-AFM nanolithography.

A listing of figure and table captions

Figure 1. Schematic illustration of electric-field-assisted contact mode AFM-based nanolithography experimental setup.

Figure 2. Voltage effect on lithography feature size. (a) Topography of lines fabricated with 32.4V, 33.3V, 34.1V, from left to right. (d) Topography of lines fabricated with voltage ranging from 22.93V, 21.18V, 23.1V, 21.35V, 23.28V, 21.53V, 23.45V, 21.7V, 23.63V, 21.88V, 23.8V, 22.05V, 23.98V, 22.23V from left to right. (b)&(e) Average height profiles of the patterns in Fig. 2(a)&(d). (c)&(f) Voltage versus feature dimensions.

Figure 3. Tip bias hold time effect on feature sizes. (a) 2D image of holes fabricated using electric-field-assisted contact mode AFM-based nanolithography. Tip bias applied was 24 V and bias hold time was 100 ms, 160 ms, 220 ms, respectively. (b) Front view of the 3D image of the holes, depths of the three holes are 5.3 nm, 8.9 nm, 11.0 nm, and widths are ~27 nm, ~31 nm, and ~33 nm, respectively. (c) Bias hold time versus dimensions of holes.

Figure 4. Force effect on lithography feature sizes. (a) Topography of NSF logos fabricated with 1 nN and 8 nN setpoint force with the same applied bias (20V). (b) Height profile of patterns in Fig. 4(a).

Figure 5. Nanopatterns fabricated with electric-field-assisted AFM lithography. Applied force is 1 nN for all the patterns.

Figure 6. Nanopatterns fabricated with electric-field-assisted AFM lithography in different speeds (50, 10, 5, 0.5 μm/s from left to right, respectively). Applied force is 1 nN for all the patterns.

Figure 7. Electric field strength distribution in the polymer film during lithography (applied tip bias = 20V). (a) Front view of the simulation model, including the location of Line 1-6. (b) Electric field distribution in the PMMA film. (c) Electric field distribution on Line 1-5. Based on the experimental results, which have feature width of around 16 nm, the relative electric field strength on the tip-sample interface (Line 1) should reach or exceed $1.63 \times 10^9\ V/m$. (d) Electric field distribution along Line 6.

Figure 8. Electric field strength distributions on the tip-sample interface (along the Y-axis) using 20 V tip bias with (a) different tip radii of 3, 5, 10, and 20 nm when PMMA film thickness is 15 nm, and (b) different PMMA film thicknesses of 10, 15, 20, and 30 nm using a tip with 35 nm radius.

Figure S1. Actual experimental setup

Figure S2. Illustration of the tip-sample distance effect on the minimum feature size in E-AFM nanolithography.

Table S1. Specifications of the AFM probes for nanopatterning and imaging.